

# Automatic Reacquisition of Satellite Positions by Detecting Their Expected Streaks In Astronomical Images.

Martin P. Lévesque

*Defence R&D Canada- Valcartier, 2459 Boul. Pie XI North, Québec, QC, G3J 1X5 Canada,  
martin.levésque@drdc-rddc.gc.ca*

## ABSTRACT

Artificial satellites, and particularly space junk, drift from their known orbits. In the surveillance-of-space context, they must be observed frequently to ensure that their corresponding orbital elements are up-to-date. Autonomous ground-based optical systems are regularly tasked to observe these objects, measure their positions, and then update their orbital parameters accordingly. The real satellite positions are provided by the detection of the satellite streaks in the astronomical images specifically acquired for this purpose. This paper presents the image processing techniques used to detect and extract the satellite positions. The methodology includes several processing steps including: image background estimation and removal, star detection and removal, an iterative matched filter for streak detection, and finally false alarm rejection algorithms. This detection methodology is able to detect very faint objects. Simulated data were used to evaluate the methodology's performance and determine the sensitivity limits where the algorithm can perform detection without false alarm, which is essential to avoid corruption of the orbital parameter database.

## 1. INTRODUCTION

With the development of the space exploitation technologies, Earth is now surrounded by thousands of orbital objects. Their number will increase in the future because new satellites are launched regularly. A high level of situation awareness is required to minimize the risk of a space collision. The recent collision between Cosmos 1951 and Iridium 11 is a reminder of the need to this type of situational awareness.

The U.S. Space Surveillance Network (SSN) has the mission to maintain an up-to-date knowledge of the orbital parameters of every Earth orbiting detectable object. External forces perturb object motion and change the orbital parameters, thus the satellites must be periodically re-observed and orbital element updates must be performed to maintain the currency of the database. These observations are performed with ground based telescopes, radars and also with optical satellites.

Canada is currently developing remotely-operated low-cost Deep Space optical sensors (Ground Based Optical project) along with automatic processing and reporting capabilities using commercially available sensors, communication and computing technologies for Surveillance of Space [1-4]. An example of such a system is a series of small COTS observatories [3] that each use 0.35m telescopes along with an Apogee CCD camera and computer controlled robotic mounts manufactured by Software Bisque. Such a system can detect satellites to magnitude 15 [5], and magnitude 16 under clear, moonless skies. This computer-controlled system can acquire hundreds of images in a single tracking session. Initial developmental issues pertaining to automatic acquisition have been recently solved and it remains to process and analyze the data collected by the sensors. The automatic detection and reporting of satellite positions is the issue addressed in this paper.

## 2. ACQUISITION PROCESS

The sensor's acquisition task is programmed with a list of resident space objects (RSO; active satellites or other space debris) which require new observations. This list is usually made up of a selection of obsolete (i.e., becoming erroneous or "stale") TLEs (Two Line Element set; a data format that contains the description of the mean orbital parameters used with Simplified General Perturbation theory). Usually the degradation rate of the orbital parameters is known and a TLE is declared obsolete when the cumulative error is above a predetermined threshold. This error must be maintained under a certain limit, ideally less than the sensor field-of-view (FOV) to ensure a successful reacquisition.

Once the task planning is completed, the sensor starts the series of acquisition. It is pointed at the appropriate time and position where the RSO is expected and one or several images are acquired. Then the algorithms detect the RSOs in the images and measure and report angles-only positions. The position accuracy is assured by the calibrated astrometry provided by the background image stars. Using this new information, new TLEs are generated and the database is updated. This observation cycle is illustrated in Fig. 1.

This acquisition procedure offers an advantage that the processing algorithms can use; the seek RSO is already known. Its exact position is not known but its angular rates and direction are. The satellite approximate brightness is also known. The satellite rotation (tumbling) is easy to measured but it is not currently recorded in the database. The angular speed and direction are used (along with the optical FOV, exposition time and pointing parameters), to predict the length and direction of the satellite streak and this information is used to develop a corresponding matched filter. Thus, the algorithms presented in this paper are algorithms developed especially for the reacquisition purpose, they are not appropriate for the detection of unexpected objects with unknown orbital parameters.

An example of an image acquired for the detection of a satellite is presented in Fig. 2. In this image, the local signal-to-noise ratio ' $SNR_{ij}$ ' ( $SNR_{ij}$  is the SNR for a single pixel while SNR is evaluated over the entire object) of the satellite streak is around 3. It is easily detected by the algorithms described below but a human observer may fail to see it, particularly if hundreds of similar images have to be inspected every day.

The streak detection is performed using a matched filter technique [6-7]. However, the performance of a matched filter without any pre-processing is quite limited and generates several false alarms. This is particularly true in presence of stars that have the properties of Dirac's delta, which always offer a good response with any matched filter. However, the nature of these images allows us to use another strategy; the negative approach. One can detect every non-streak object (i.e., a star) that is easy to detect and erase these objects until only the 'yet undetected' streak remains. This is the processing scheme illustrated in Fig. 3.

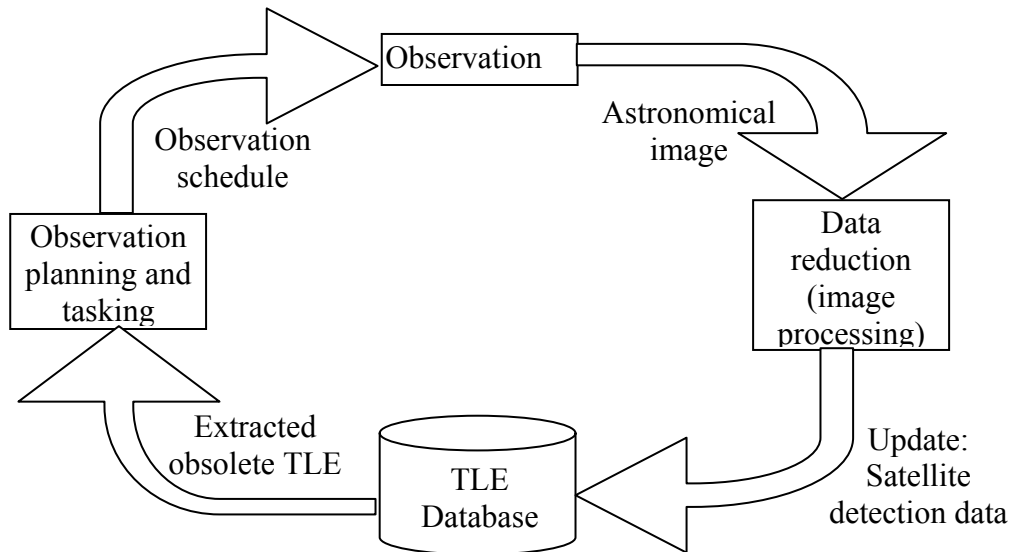


Fig. 1. Observation cycle showing how an old TLE generates an observation task that will be used to update the database.

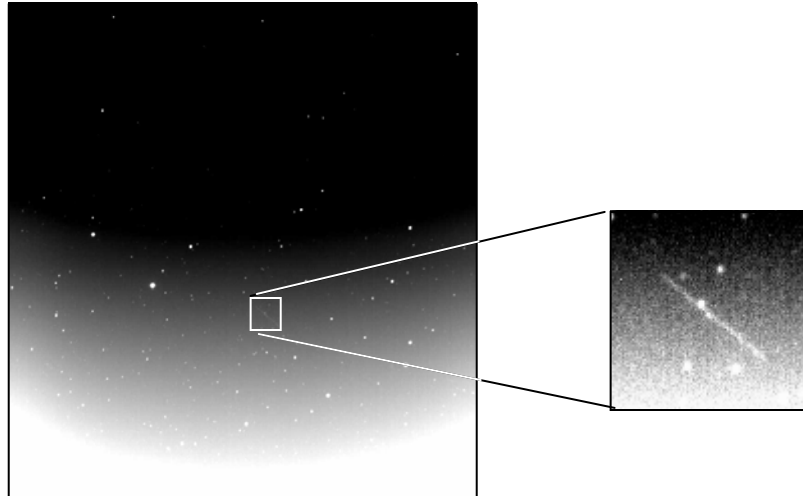


Fig. 2. An example of an image acquired for the detection of a satellite.

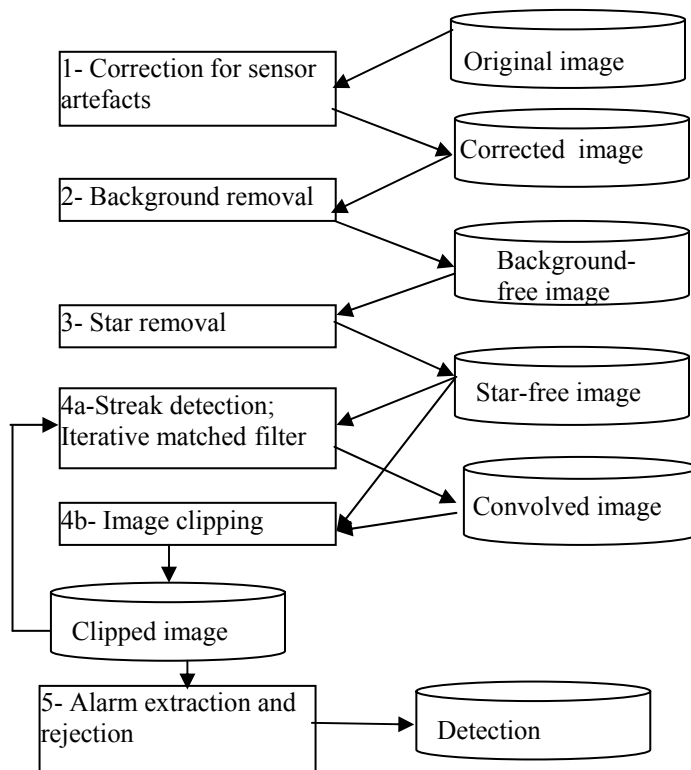


Fig. 3. – Overview of the detection processing

### 3. DETECTION ALGORITHMS

The processing begins with the correction of the sensor artifacts (dead pixels). Then the accurate image background is estimated and subtracted. After, the stars are detected and erased. This process is tricky because the streak must not be altered during this step and the star-erase process must not leave residue artifacts. Once the image is clear of undesirable objects, the matched filter is applied. This leaves false alarms that most of the time can be easily discarded. Thus, the image is segmented into individual objects which are analyzed and rejected if they do not show the expected characteristics. Finally, for the remaining alarms, the detection confidence levels are evaluated and the

ranked detections are reported. In this processing sequence, four steps require special attention because ad hoc algorithms were developed specifically for this purpose. They are the background estimation, the star detection and erasing process, the ‘iterative’ matched filter and finally the false alarm rejection algorithms (steps 2 to 5 in Fig. 3).

The image background is a nuisance for the detection algorithms. It must be removed. The most popular method consists of acquiring and subtracting a dark frame, i.e., an image acquired with the same conditions of CCD temperature and exposition time but without a signal (the shutter remains off). However, [8] demonstrates that this method is not accurate enough because it leaves a background residue with an amplitude higher than the noise level. The main cause is small temperature variations over the CCD. Furthermore, this method augments the dark frame noise to the acquired image.

The iterative background removal method [6] and [8] offers better results. This method assumes that the background is smooth while the other objects are sharp. The method may fail in presence of bright nebulae but it is very accurate otherwise. In effect, the local image average pixel value is already a good background estimation. This average can be obtained with polynomial fit [6] or with local statistics (local means and standard deviations) [8]. However, this average is corrupted by the presence of bright objects. So, the image values above this average (plus a noise tolerance margin) are clipped and the average is calculated again with a reduced corruption. After several iterations, an excellent estimation of the background is obtained. It is estimated in [8] that the left-over background residue is less than the 1/5 of the noise level, which is better than other tested commercial methods. The background removal efficiency can be seen in Fig. 6B and 6C.

The next step consists of detecting and erasing stars, without affecting the streaks. As indicated in [6], the detection is performed with the double gate filter illustrated in Fig. 4. The stars are detected when the average signal in the inner window ( $\mu_{in}$ ) is high above the noise level ( $\mu_{in} > 3\sigma_n$ ) while the outer window measures only the background ( $\mu_{out} < 2\sigma_n$ ). A streak is present simultaneously in both inner and outer windows and cannot respect these two conditions. Hence, a streak is not detected, nor erased. However, to avoid the erasing a faint streak, one detected in the inner window but not in the outer window, the sensitivity of the outer window (which contains more background pixels) needs to be increased. The external window is separated into several windows with the same size as the inner window. If any one of these outer windows detects a signal, then the detection is canceled, as this may be a streak, not a star.

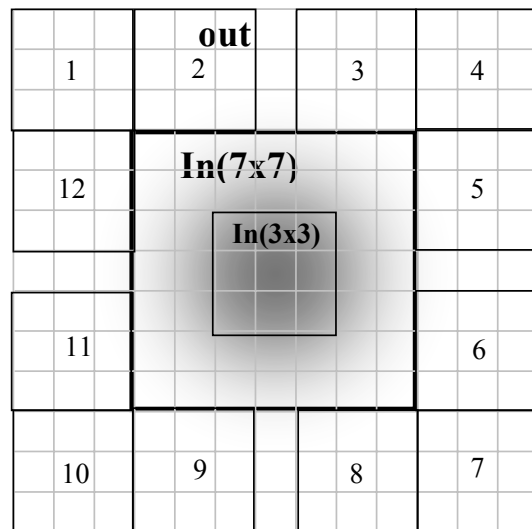


Fig. 4.- Star detection filter with streak rejection capability designed for a PSF width of 3 pixels at half height.

Some very bright stars may deceive this filter. Because of the shape of the PSF function, a part of the object energy is spread into the outer window. Therefore, an additional detection rule is required; the PSF peak must be significantly brighter than the average background, i.e.:  $\mu_{in} > 10\mu_{out}$ . The combination of these two rules produces the following detection rules:

$$\text{Star detected if: } [\mu_{in} > 10\mu_{out}] \text{ or } [(\mu_{in} > 3\sigma_n) \text{ and } (\max(\mu_{out-k}) < 2\sigma_n)] \quad (1)$$

However, this filter is not perfected yet. Because of a sensor blooming artifact, the brightest stars have larger than normal PSF. The size of the gap between the inner and outer windows must be increased for bright stars. For faint stars, the central gap is twice the normal PSF width, i.e. it is the 7x7 pixels window indicated in Fig. 4. For very bright stars (close to the saturation) the size of this gap is double, i.e., the central gap becomes 13x13 pixels and it is surrounded by 20 3x3 outer windows. The result of this filter is illustrated in Fig. 6D where all detected stars are copied into this image plane.

Once a star is detected, it must be erased from the image. Because of the PSF width and the area affected by the star, the erasing process is not simple. The central group of pixels cannot simply be set to zero, this leave a halo shape artifact, which is harmful for the detection [6]. The area where the pixels contain measurable signal from the star extends several PSF widths from the central point. Thus, the star profile must be measured and subtracted from the image. This measurement is done by applying a median filter on groups of pixels having an equivalent distance 'r' from the star central point. This provides the most probable value for the star intensity 'I(r)' as a function of the radius. This function is subtracted as far as six PSF widths from the central point. Finally only the central pixels, inside a radius of two-PSF, are set to zero. This method completely erases a star without leaving an artifact and without affecting nearby objects. Once a maximum of stars are erased, the streak detection matched filter has a much better chance of success. This can be seen in Fig. 6E where only the pairs of stars (or a combination of stars and background or noise residue) remain.

With the observation cycle shown in Fig. 1, the speed and direction of the seek satellite are known parameters. A matched filter can be design to detect the satellite. First, the image astrometry needs to be known. The image pointing and orientation are approximately known with the telescope pointing parameters. But it is the recognition of the stars in the observed field of view that provides the best pointing reference. This is done with commercial software like PinPoint™ developed by 'DC-3 Dreams' [9]. Once the astrometry is accurately known, the satellite TLE is used to calculate two expected positions; at the instant the camera shutter opened and when it closed. The positions are converted into pixel coordinates and they define the endpoints of the equivalent line segment that represents the expected streak. This line segment is the template used for the detection (i.e., to design the matched filter). It is generated with a normalized intensity (sum of all pixel values equal one), so it is easy to relate the intensity of the convolution peak to the mean object intensity.

A first iteration is obtained by convolving the image (with background and stars removed) by the line-segment template. This is done with the Fourier transform method. The result is illustrated in Fig. 6G. Unfortunately, some very bright stars (brighter than the streak) produce strong false alarms. However, the inspection of values and shapes of the convolution peaks is interesting. The streak (a rectangle function) convolved with the line segment template (a normalized rectangle function) provides a peak with a triangular shape. The maximum intensity of the convolution peak is the average streak intensity. This is illustrated in Fig. 5. But for a star (a Dirac's delta function), the result is completely different; the total intensity of the convolution peak is severely attenuated because the convolution kernel overlaps a large background area around the star.

This suggests that the intensity of the convolution peak could be used to blindly clip the original signal; the streak would be preserved while the remaining stars would be attenuated. After clipping, the signal could be convolved again because the streak remains unchanged while the stars are attenuated. This idea is the principle of the iterative matched filter developed for streak detection. Firstly, one can think of building a clipping mask where the convolution peaks are replaced by calibrated line segments (with intensity set by the value of the corresponding convolution peak). But there is a simpler solution. Fig. 5 suggest that twice the intensity of the convolved image will do the job. The clipped image is simply the minimum between the image before convolution and the convolved image multiplied by two, i.e.:

$$I_{n+1} = \min (I_n, 2(I_n \star \text{streak\_template})), \quad (2)$$

where '⋆' is the convolution operator. Fig. 5 indicates that this relation preserves the streak shape but it clips the stars. This also replaces the high noise values by the mean noise value in the rest of the image, enhancing the alarm contrast. Fig. 6H shows this first clipped image (with an increased contrast). The number of false alarms is lower

and the noise is reduced. Figure 6I and 6J show the image convolved a third time and the image after the third clipping. The streak is still preserved and the number of false alarms reduced further. After three iterations, the improvements are less significant but the detection performance continues to improve slightly. A maximum of 12 iterations were tested, above which no improvement is visible. With the presented image, the streak becomes the strongest signal after three iterations, but this is a quite bright streak. Its  $SNR_{ij}$  is above 3. However, this filter has the capability to detect fainter streaks (with  $SNR_{ij}$  lower than 1) and, in these cases, the 12 iterations are desirable.

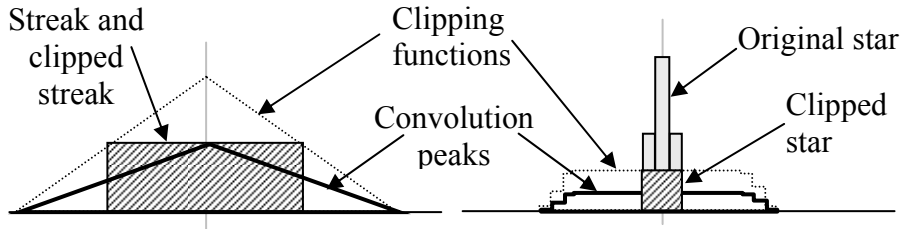


Fig. 5. Shape of the objects (star and streak), their convolution peaks and clipping functions.

#### 4. FALSE ALARM REJECTION

After the application of the iterative matched filter, some false signals will always remain. Their morphologies indicate clearly that most of them are false alarms, but a simple intensity threshold cannot extract the real detection among them. Therefore, the alarms are individually extracted (Fig. 6L) and further analyzed. This is done with the extraction mask of Fig. 6K, which is a threshold version of the last convolved image (Fig. 6I). The convolution peaks (with their shape and size) indicate where the groups of pixels of interest must be isolated and extracted. A certain number of sub-images are created, containing only one alarm each. Then a number of parameters are evaluated to determine the nature of the objects. There are the moment of intensity (like the moment of inertia, but calculated with the pixel intensity), the ratio between the moments of intensity of the two principal axis (parallel and perpendicular to the streak direction), length and orientation of the object and the SNR. The details of the extraction method and parameter evaluations are provided in [7].

For relatively bright objects ( $SNR_{ij} > 1$ ), the object compactness given by the moment ratio is useful for the discrimination between pairs of stars and a real streak. For a single star, this ratio is exactly one (a compact object with no privileged direction). Pairs of stars (those that eluded the star detection filter) have small moment ratios, typically between 1 and 10. Streaks always have higher moment ratios, typically above 100. In these cases, the set level for the moment ratio threshold is obvious, at least for bright objects. However, because maximum sensitivity is desired, fainter and fainter objects (corrupted by noise) need to be detected and the discrimination provided by the moment ratio decreases with the SNR. In this case, at low SNR values, there is another parameter that has proven to be more stable and straightforward to evaluate; this is the ratio between the length of the extraction mask (or length of the convolution peak) and the expected length of the streak (defined in the matched filter). Thousand of analyzed alarms showed that the streak extraction mask is always longer than the length of the expected streak (because of the triangular shape of this convolution peak), which is never the case for the extraction mask of other objects. This can be seen in Fig. 6K. Following a convolution, streaks tend to have triangular peaks twice as long as the initial streak, while other objects (point sources or close-by star pairs) tend to have much shorter and flatter peaks. The discrimination capability of this criterion reaches its limits when the SNR is so faint that it cannot realize the difference between real streaks and random noise patterns. So the SNR of the extracted object is itself a criterion that needs to be evaluated to limit the generation of false alarms. Also, for a stable and accurate measurement, the SNR is evaluated over the standard object area (the same for all alerts). It is measured over an equivalent streak area, so the SNR of different alerts can be compared. In summary, a combination of SNR, moment and length ratio is used to determine when an alert is a streak or not.

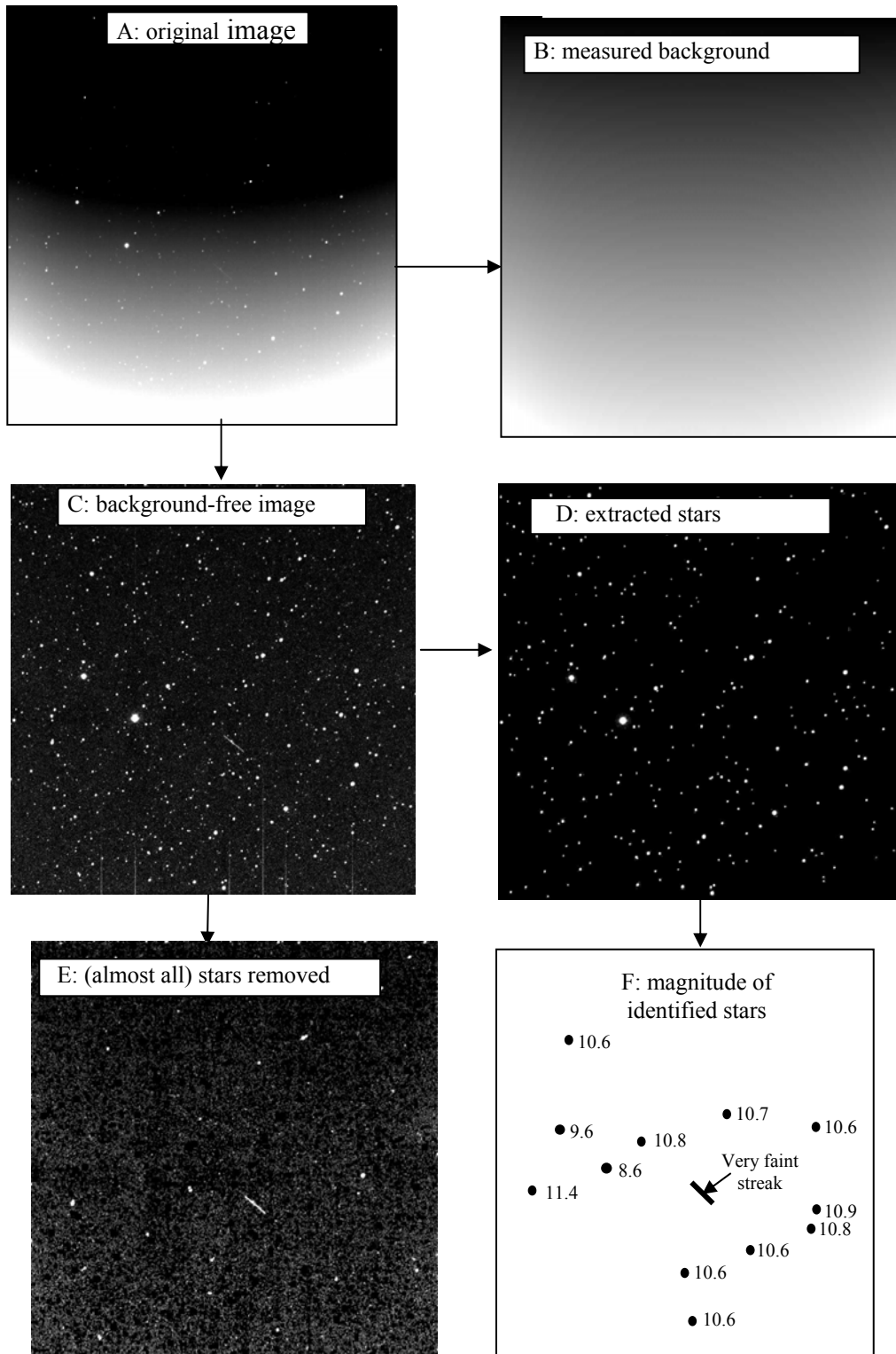


Fig. 6.- Processing sequence for the detection of the satellite streak: A: original image, B: estimated background, C: background free image, D: detected stars, E: image without stars, F: identified stars (for astrometric and photometric calibrations).

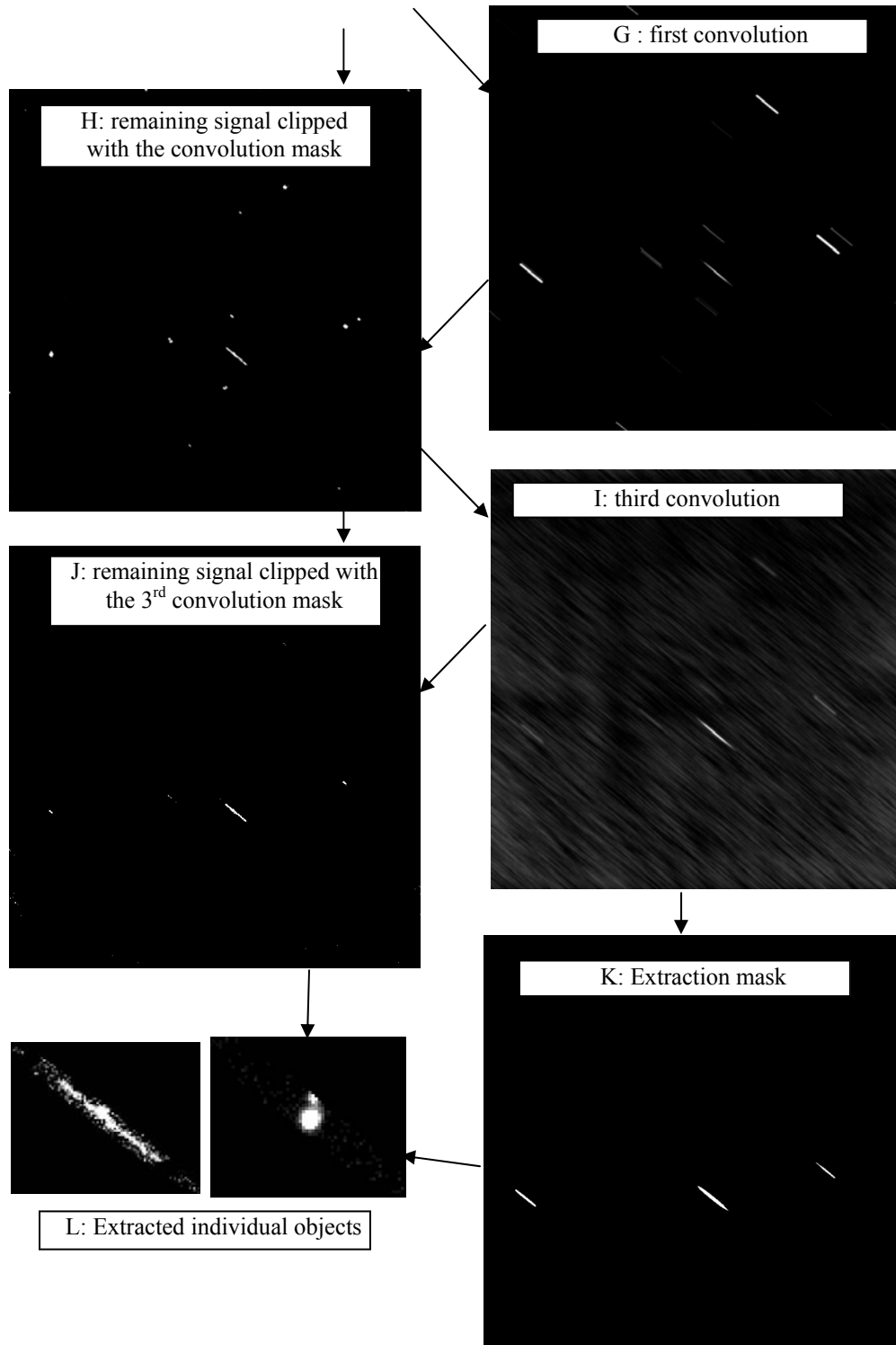


Fig. 6. (Continued) – G: first convolved image, H: first clipped image, I: third convolution iteration, J: third iteration of image clipping, K: object extraction mask and L: individual extracted alerts.

## 5. PERFORMANCE EVALUATION

The detection algorithms were encoded in Matlab™. The program reports the alarms along with several measured parameters like the SNR,  $SNR_{ij}$ , length ratio, momentums and other parameters. It also includes a model of the probability of detection functions (PDF) that were obtained by analyzing the detections performed with thousand of simulated images (Fig. 7). When a detection is declared, an estimate of the PDF is provided, indicating the degree of confidence in the result. The algorithm can detect a streak as faint as  $SNR_{ij} = 0.5$ , i.e., a streaks where the mean intensity is only half the noise level. However, the streak is an extended object and after the integration of the signal over the entire area, a streak with 100 pixels has a total  $SNR = 5$ , which is easily detectable with a matched filter.

Thousand of simulated images (containing stars, pairs of stars and streaks of various length and intensity) were generated for the performance testing. The objects were generated with controlled photon and CCD noise and optical PSF. Because the characteristics of the simulated detected object are precisely known, it was possible to draw exactly the figure of performance. Real astronomical image were also used to confirm the detection capability and reliability of the algorithms, but because of the uncertainty on the measurement of the object brightness (when  $SNR_{ij}$  is lower than 1), they were not used for the PDF evaluation.

Fig. 7 indicates the detection performance measured with these simulations. The PDF presented in Fig. 7 is the net PDF, not the raw PDF. A raw PDF simply means the capability to detect a target when a target is present in the image, without considering the confusion created by the presence of false alarms. In fact, the matched filter technique is so sensitive that a streak with a  $SNR_{ij}$  as low as 0.1 is incredibly always present in the list of possible detections, but the algorithm system fails to report it because there are always stronger false alarms. A net PDF is the probability of declaring a target without confusion after the elimination of all other false alarms. This is the plot reported in Fig. 7. Hence, the detection algorithms presented above have almost a PDF of 100% for a long streak (130 pixels) with a  $SNR_{ij} > 0.5$ . This is very good performance. This is 6 times fainter than the streak presented in Fig. 2. The performances are better for long streaks, which is not unexpected because this is the characteristic that provides the discrimination capability of the matched filter.

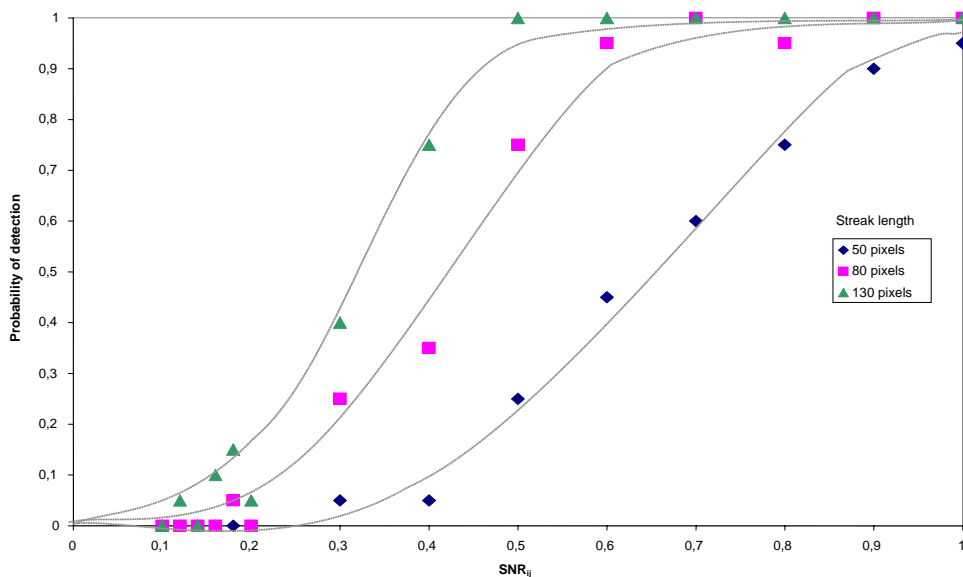


Fig. 7.- Net probability of detection of streak of various streak lengths.

## 6. CONCLUSION

The processing described in this paper identifies several processing algorithms used for the automatic detection, which completes the automatic observation loop; tasking, acquisition, detection and TLE update. These detection algorithms always detect satellite streaks without false alarm when they are brighter than the noise level ( $SNR_{ij} > 1$ ) and when they are long enough ( $> 80$  pixels). For longer streaks ( $> 130$  pixels), they are reliable for  $SNR_{ij} > 0.5$ . These calibrated results were obtained with simulated images, which included objects with known properties. They were thereafter confirmed with the processing of real images [7]. The performance of the detection algorithms was modeled and an estimation of the detection reliability (PDF) is reported along with the detection. Hence, the detection of bright enough streaks is fully automatic because they are declared with a score of 100%. For streaks with lower brightness, the report indicates the detection may need to be confirmed by the analyst. For very faint streak, a cueing mode is also provided (for streaks as faint as  $SNR_{ij} = 0.2$ ) where the detection is indicated along with other false alarms. It is possible that an analyst could visually confirm such detections, but most of the time he would not have himself noted the presence of such a faint satellite in the imagery. For streaks with lower  $SNR_{ij}$ , in the range of 0.1 to 0.2, the simulation demonstrated that the algorithms are (most of the time) able to indicate the target in a list of possible detections, but the analyst would not necessarily be able to see and confirm them anymore.

## 7. REFERENCES

1. Earl, M and Racey, T. (2000). "The Canadian Automatic Small Telescope for Orbital Research (CASTOR) A Raven System in Canada", [http://www.rmc.ca/academic/physics/castor/castor1\\_e.html](http://www.rmc.ca/academic/physics/castor/castor1_e.html) , accessed April 2008.
2. Kervin, P., "RAVEN Automated Small Telescope Systems," AFRL Directed Energy Directorate, Optical and Imaging Division, Space Surveillance Systems Branch, 2000.
3. Wallace B., Rody J., Scott R., Pinkney F., Buteau S., Lévesque M. P., "A Canadian Array of Ground-Based Small Optical Sensors for Deep Space Monitoring", 2003 AMOS Technical Conference.
4. Wallace, B., "The DRDC Ottawa Space Surveillance Observatory", AMOS Technical Conference 2007, Maui HI.
5. Scott R. and Wallace, B., 'Small Aperture Optical Photometry of Canadian Geostationary Satellites', Canadian Aeronautics and Space Journal, 2009.
6. Lévesque M. P., Buteau S., Image Processing Technique for Automatic Detection of Satellite Streaks. DRDC Valcartier 2005 TR-386. Defence R&D Canada – Valcartier. <http://cradpdf.drdc.gc.ca/PDFS/unc64/p527352.pdf> , accessed Feb. 2009.
7. Lévesque M. P., Lelievre M., Improving satellite-streak detection by the use of false alarm rejection algorithms. DRDC Valcartier TR 2006-587. Defence R&D Canada – Valcartier. <http://pubs.drdc.gc.ca/PDFS/unc76/p530206.pdf> , accessed Feb. 2009.
8. Lévesque M. P., Lelievre M., Evaluation of the iterative methods for image background removal in astronomical images. DRDC Valcartier TN 2007-344. Defence R&D Canada – Valcartier. [http://pubs.drdc.gc.ca/PDFS/unc69/p52905\\_4.pdf](http://pubs.drdc.gc.ca/PDFS/unc69/p52905_4.pdf), accessed Feb. 2009.
9. <http://pinpoint.dc3.com/> , accessed Feb. 2009.